

Particle motion trajectory tracking based on fiber optic tweezers*

ZHAO Cun¹, DONG Taiji^{2**}, GAO Bingkun², LIU Xu², and ZHANG Zihua³

1. Department of Electrical Information Engineering, Northeast Petroleum University Qinhuangdao Campus, Qinhuangdao 066004, China

2. College of Electrical and Information Engineering, Northeast Petroleum University, Daqing 163318, China

3. Faculty of Materials and Manufacturing, Beijing University of Technology, Beijing 100124, China

(Received 18 December 2022; Revised 17 February 2023)

©Tianjin University of Technology 2023

A biosensor based on single-fiber optical tweezers is proposed, which can detect the motion trajectory of cells based on the stable capture and transmission of silica microspheres as well as biological yeast cells by using a tapered optical fiber as a sensing element. The interference cavity is formed by using the fiber tip and the target particle, the detected interference signal is demodulated using Hilbert transform, and the displacement curve of the particle is plotted to realize the particle motion trajectory tracking. This method provides potential technical support for process monitoring of targeted drug delivery in biomedicine.

Document code: A **Article ID:** 1673-1905(2023)08-0462-6

DOI <https://doi.org/10.1007/s11801-023-2215-x>

In recent years, the development of science and technology has progressed from macroscopic to microscopic scales, and therefore the manipulation of tiny-sized objects has become increasingly important in the fields of micro and nano sciences, materials chemistry, and biomedicine^[1]. Traditional manipulation techniques are based on contact mechanical gripping, such as miniature robotic arms, tweezers, and probes^[2-4], which inevitably cause deformation and other effects on the manipulated objects, thus causing damage to the manipulated objects and even irreversible active damage to living materials. With the rapid development of fiber optic technology, the introduction of fiber optic devices has greatly improved the freedom and flexibility of optical tweezer systems, and fiber optic optical tweezers have become another powerful tool for exploring the microscopic world. Fiber optic optical tweezers are more suitable for particle manipulation because they confine the spatial activity of the target particle by the gradient force of the optical local field as opposed to the direct contact mechanical tweezers, which are non-contact and gentle manipulation. Typically, light emitted from the tip of an optical fiber diverges, and a stable optical trap can only be achieved by balancing the gradient and scattering forces of two opposing fibers. Therefore, multiple fibers are required to form a conventional single optical trap. Based on the development of microfabrication techniques at the end of optical fibers, the three-dimensional optical force generated by forming the fiber tip into a special conical shape

to trap biological particles marks the emergence of single-fiber optical tweezers^[5]. Based on the common single-fiber tweezer, it is easier to study and control, and power transmission and distribution is easier than control^[6,7]. As a result, many structures have been rapidly developed, such as narrow parabolic tapered-tip fiber optical tweezers^[8], reflection-based tweezers axial taper tip fiber optic optical tweezers^[9], high refractive index fiber optic optical tweezers^[10], and multi-core fiber optic optical tweezers^[11,12]. However, most of these methods have problems such as high fiber optic cost, difficult production and tedious operation. Moreover, due to the development in the field of micro-operation^[1], more and more demands are made on the functionality of fiber optic optical tweezers. In the process of stable particle capture and transport, it is often critical to monitor the state of particle motion as well as the transport distance. How to integrate multiple functions on the same fiber to realize multiparameter sensing fiber has become an urgent problem.

To solve the above problems, a sensor based on single fiber optical tweezers is proposed in this paper, and a tapered fiber probe for capturing silica and yeast biological cells is prepared by fusion heating and stretching, and stable capture and manipulation of silica microspheres and yeast biological cells is successfully achieved. Moreover, the high sensitivity property of the swift field exposed by the tapered fiber tip is used to make the fiber tip a sensitive sensing element. When the cell is displaced, the interference signal

* This work has been supported by the National Natural Science Foundation of China (No.61422301).

** E-mail: dongtaiji_nepu@126.com

is generated due to the change of the outer cavity length, and the interference signal is demodulated using Hilbert's algorithm, which in turn enables the monitoring of the motion state of the particle during transportation.

The laser beam focused by the lens exerts a force on the particles near its focus. From the dipole model of dielectric, this force can be divided into two categories, one is called scattering force, the effect of scattering force on the particle from the light in the scattering process and the photon momentum exchange, the particle makes the photon momentum change, and in turn the particle itself by the momentum change of the reaction force, the direction of the scattering force along the direction of light propagation, the effect of the particle along the direction of light propagation, and the effect is to make the particle move along the direction of light beam propagation. The other category is called gradient force (gradient force), the gradient force on the particle comes from the electric dipole moment in the dielectric sphere in the inhomogeneous electromagnetic field by the force, it is proportional to the gradient of light intensity, pointing to the maximum intensity of the light field. Its effect causes the particle to move toward the point of maximum optical power density. The optical tweezers are formed because the gradient force generated by the laser is greater than the scattering force, thus capturing the particles near the center of the focused spot.

When a high-intensity laser beam is directed at a dielectric particle, the momentum transfer of the incident photon scattering will exert an optical force on the particle near the focus. The resulting optical force traditionally consists of two components, the scattering force and the gradient force. The Rayleigh scattering condition will be satisfied when the wavelength of the laser beam is much larger than the size of the captured particles. Under these conditions, the optical force can be obtained by treating the particle as a point dipole. For a particle of radius a , the scattering force is given as follows

$$F_{\text{scatt}} = \frac{I_0 \sigma n_m}{c}, \quad (1)$$

$$\sigma = \frac{128\pi^5 a^6}{3\lambda^4} \left(\frac{m^2 - 1}{m^2 + 2} \right)^2, \quad (2)$$

where I_0 is the intensity of the incident light, σ is the scattering cross section of the particle, n_m is the refractive index of the surrounding medium, c is the speed of light in vacuum, m is the ratio of the refractive index of the particle to the refractive index of the medium (n_p/n_m), and λ is the wavelength of the captured laser. The scattering force is in the same direction as the incident light and is proportional to the intensity of the light. The optical gradient force is generated by the interaction between the induced dipole and the non-uniform field as

$$F_{\text{grad}} = \frac{2\pi\alpha}{cn_m^2} \nabla I_0, \quad (3)$$

$$\alpha = n_m^2 a^3 \left(\frac{m^2 - 1}{m^2 + 2} \right). \quad (4)$$

When the size of the captured particle is comparable to the wavelength of the captured laser beam, in which case the electric dipole method is ineffective, numerical simulation and computational methods based on electromagnetic theory, such as the finite element method and the time-domain finite difference method, can be used for the calculation of the optical force. The combined force (F_O) applied to the particle can be calculated by computing the integral of the time-independent Maxwell stress tensor ($\langle T_M \rangle$) along the total outer surface of the particle, where $\langle T_M \rangle$ can be written as

$$\langle T_M \rangle = \mathbf{D}\mathbf{E}^* + \mathbf{H}\mathbf{B}^* - 1/2(\mathbf{D} \cdot \mathbf{E}^* + \mathbf{H}\mathbf{B}^*)\mathbf{I}, \quad (5)$$

where \mathbf{D} and \mathbf{H} are the potential shift and magnetic field, respectively, \mathbf{E}^* and \mathbf{B}^* are the complex conjugates of the electric field \mathbf{E} and magnetic field \mathbf{B} , respectively, and \mathbf{I} is the isotropic tensor. The combined force on the particle is

$$F_O = \oint_S (\langle T_M \rangle \cdot \mathbf{n}) dS, \quad (6)$$

where \mathbf{n} is the surface normal vector.

Simulations are performed by using the fluctuating optics module (electromagnetic waves, frequency domain) of a commercial finite element simulation software and boundary conditions of a perfectly matched layer for the electric field distribution at the fiber tip and the magnitude of the forces on the particles in the optical tweezers experiment. Boundary-mode analysis is used for the analysis of the transport modes. Parametric scanning is used to calculate the forces on the particles at each position in the electric field. The refractive indices of the fiber, particle, and water were set to 1.45, 1.45, and 1.33, respectively, and the particle diameter was set to 5 μm . The wavelength was set to 980 nm, and the input power was set to 1 W/m, as shown in Fig.1. We analyzed the electric field distribution at the tip of the fiber when the particle was at 37 μm , 39 μm , 41 μm , and 43 μm . From Fig.1, it can be seen that the focal length is further extended as the distance between the sphere and the fiber tip increases. At this point, the force on the particle at different positions is different, and further analysis of the force on the particle is needed in order to derive a stable capture point for the particle.

To numerically simulate the non-contact capture capability of fiber optic optical tweezers, in this paper, we used the parametric scanning module in COMSOL software to calculate the forces on particles in the range of 34–46 μm , and we calculated the optical forces on a single microsphere (5 μm in diameter). The radial and axial force distributions of the microspheres were obtained by integrating the time-independent Maxwell stress tensor (T_M) over the enclosed surface of the particles. It can be seen from Fig.2(a) that the force on the particle is positive before 36.6 μm , pushing the particle to the stable capture point. In the range of 36.6–37.8 μm ,

the force on the particle is negative, which pulls the particle toward the stable capture point and is expressed as the capture gradient force. After $37.8 \mu\text{m}$, the force on the particle is positive and is expressed as a scattering force. When $x=37 \mu\text{m}$, the force analysis of the particles along the longitudinal direction is performed. The light field distribution is symmetric in the longitudinal direction, so the particle force exhibits centosymmetry. When the particle is deflected in the $-y$ direction, the particle is subjected to an upward pulling force, which pulls the particle back to the axial direction. When the particle is deflected in the $+y$ direction, the particle is subjected to a downward pulling force, which pulls the particle back to the axial direction. The force diagram is shown in Fig.2(b).

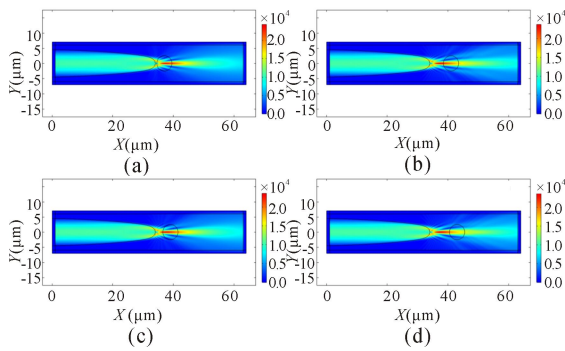


Fig.1 Electric field distributions at the fiber tip when the microsphere is at different positions: (a) $x=37 \mu\text{m}$; (b) $x=39 \mu\text{m}$; (c) $x=41 \mu\text{m}$; (d) $x=43 \mu\text{m}$

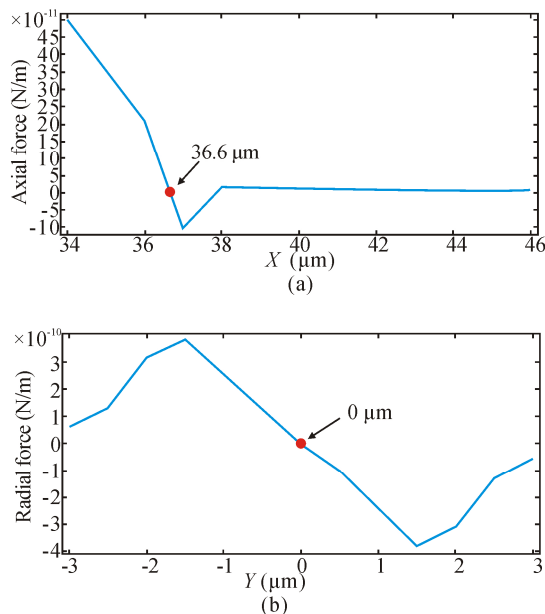


Fig.2 Magnitudes of the axial force and radial force applied to the microspheres: (a) Axial force; (b) Radial force

The fiber optic probes were fabricated by flame heating technique using commercial single-mode fiber (core diameter: $9 \mu\text{m}$, cladding diameter: $125 \mu\text{m}$). The fibers were first stripped of their buffer layer and polymer

jacket by using a fiber stripper with a stripping length of 5 cm . To prevent their breakage and warpage, the fibers were wrapped with stainless steel capillaries (outer diameter: 1.1 mm , wall thickness: 0.1 mm , length: 100 mm). The fiber was heated for about 30 s to reach the melting point, and then stretched at an initial speed of about 2 mm/s . The fiber diameter was reduced from $125 \mu\text{m}$ to $20.6 \mu\text{m}$ over a length of 2.48 mm . The stretching speed was then accelerated and stretched at a speed of approximately 20 mm/s . The fiber broke into a circular arc shape with a diameter of $2.5 \mu\text{m}$. Finally, the stretching was completed by gently wiping the fiber tip using a cotton towel moistened with alcohol, and the stretched fiber is shown in Fig.3.

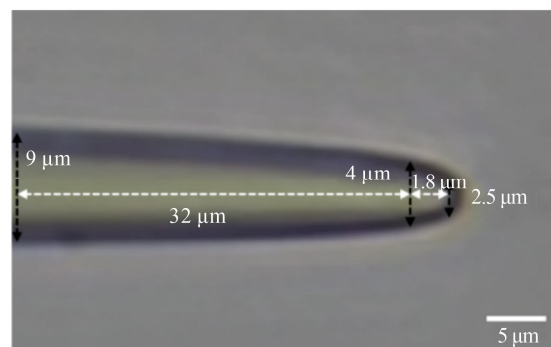


Fig.3 Fiber optic probe microscopy image

Based on the above analysis, the experimental setup was designed and built in this paper (Fig.4). The experimental images were acquired by an optical microscope through an integrated charge-coupled device (CCD), and the images were observed and recorded in real time on a computer. A laser beam with a wavelength of 980 nm was emitted into a modified tapered fiber with a power adjustment range of $0\text{--}25 \text{ mW}$. Considering the importance of the power magnitude for particle stability capture, the output power at the fiber end in the experiment was about 10 mW , and the modified tapered fiber was wrapped with a capillary tube and fixed with a three-dimensional six-axis robotic arm. During the experiment, the slides and coverslips were placed and fixed on a three-dimensional precision bench. A square cavity of about 2 cm in length and $1\text{--}2 \text{ mm}$ in height is formed between the cover glass and the slide to attenuate the Brownian motion of particles in the solution and the evaporation force of the solution in air with the help of blue gel. A portion of the solution is removed with a syringe and gently pushed into the lumen until the solution fills the lumen. Then, the tip of the conical fiber covering the capillary is fixed on the five-dimensional platform and adjusted to the same height as the solution. After that, the fibers were extended from one side into the solution for particle capture. In this experiment, $3\text{--}6 \mu\text{m}$ yeast cells as well as silica microspheres were used as capture objects.

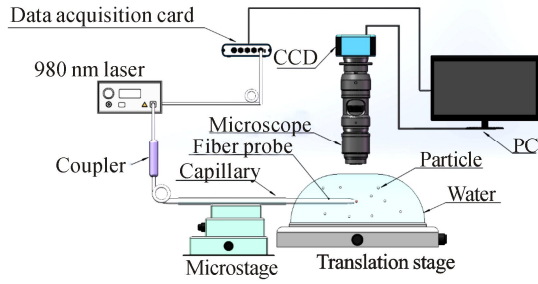


Fig.4 Single fiber optical tweezer experimental setup

We used a drawn tapered fiber probe to conduct the capture experiment of silica spheres with a diameter of $5\ \mu\text{m}$. When $t=0\ \text{s}$, the fiber probe was moved to the vicinity of the $5\ \mu\text{m}$ silica spheres (the yellow circle in Fig.5(a) represents the $5\ \mu\text{m}$ spheres, and the red circle represents the $7\ \mu\text{m}$ spheres, which were compared with the $5\ \mu\text{m}$ spheres), and at $t=1.0\ \text{s}$, the $980\ \text{nm}$ laser was turned on. At this time, the $5\ \mu\text{m}$ spheres were captured at the fiber tip, and when $t=2.0\ \text{s}$, the $5\ \mu\text{m}$ spheres were still captured at the fiber tip, while the $7\ \mu\text{m}$ spheres, due to the scattering force larger than the gradient force, were gradually pushed away. As in Fig.5(d), when $t=8.0\ \text{s}$, the $7\ \mu\text{m}$ spheres were pushed out of the imaging field of view. To verify that the silica spheres were captured at the fiber tip by the optical force, we turned off the laser at $t=10\ \text{s}$ and found that the $5\ \mu\text{m}$ silica spheres fell from the fiber tip, verifying that the spheres were captured at the fiber tip because of the effect of the optical force.

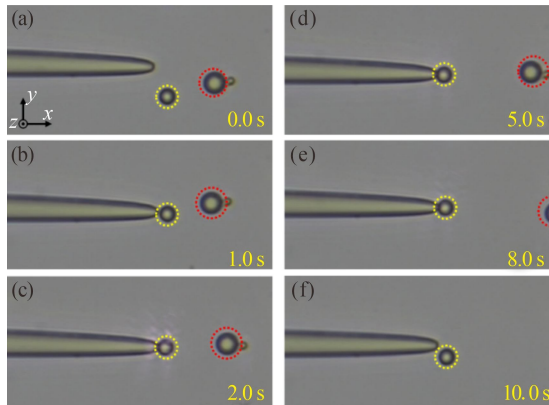


Fig.5 Schematic diagram of silicon dioxide sphere capture experiment

Furthermore, we also conducted yeast cell capture experiments, the cell samples were used for household pasta yeast cells, yeast cell suspension was made by 5% glucose solution, yeast cells were ellipsoidal, about $2\text{--}6\ \mu\text{m}$ in diameter and $5\text{--}30\ \mu\text{m}$ in length, as Fig.6 shows the yeast cell capture process, at $t=0\ \text{s}$, yeast cells with diameter about $5\ \mu\text{m}$ and length about $7\ \mu\text{m}$ were captured at $t=0\ \text{s}$, yeast cells with a diameter of about $5\ \mu\text{m}$ and a length of about $7\ \mu\text{m}$ were captured at the tip of the fiber, and then the fiber was moved up and down, and the yeast cells moved with it, as in Fig.6(b) and (c), at $t=23\ \text{s}$, we moved the fiber back and forth, and the

yeast cells also moved back and forth with the tip of the fiber to achieve the manipulation of yeast cells.

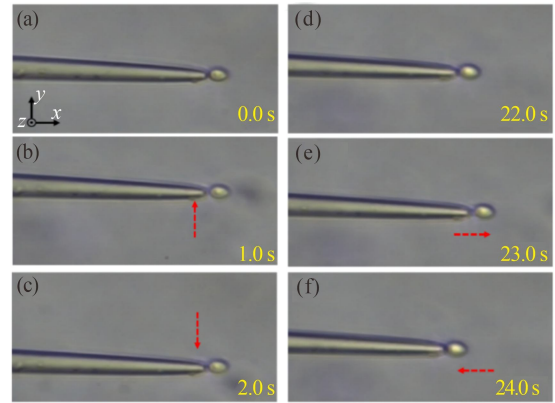


Fig.6 Schematic diagram of yeast cell capture experiment

In the process of particle transport, the velocity of particle motion and the size of particle displacement are the object parameters that characterize the particle motion state. To analyze the particle motion state, a particle displacement detection method is proposed for the detection of particle displacement. The microsphere surface and the fiber end surface can be regarded as a non-intrinsic F-P interference model, because the reflectivity of the fiber end surface is about 4%. Therefore, we can ignore the phenomenon of multiple reflections in the fiber end surface, at this time, the light feedback from the fiber end surface and the microsphere surface feedback can be approximated as a two-beam interference, the power equation can be expressed by Eq.(7). At this time, the particle movement will lead to changes in the length of the external cavity, the light from the fiber end surface irradiated to the particles after the Fresnel reflection, coupled into the fiber summary by the fiber end surface again, and in the light end surface directly. The reflection of that part of the light wave occurs interference, when the optical range difference changes, the resulting interference fringe will also change, the resolution of the interference fringe is half a fringe, that is, when the particle moves a distance of half a wavelength, corresponding to an interference fringe.

$$P(t) = P_0[R_1 + R_2 - 2\sqrt{R_1 R_2} \cos(\varphi(t))], \quad (7)$$

where P_0 represents the incident light power, R_1 and R_2 represent the reflectance of the fiber end face and the microsphere, respectively, and $\varphi(t)$ represents the phase of the interfering light, denoted as

$$\varphi(t) = \frac{4\pi n L(t)}{\lambda}. \quad (8)$$

When the cell is moved by the scattering force, the interference signal detected by the photodetector encapsulated in the laser is shown in Fig.7(a), and in order to filter out the phase noise introduced during the experiment due to the influence of the external environment, we used a Butterworth low-pass filter with a cutoff frequency of $300\ \text{Hz}$ to filter the original signal, and the

filtered interference signal is shown in Fig.7(b), and in order to reconstruct the displacement size, we used the Hilbert transform in Ref.[13] to reconstruct the signal. Firstly, we performed Hilbert transform on the original signal, from the nature of Hilbert transform, as shown in the following equation

$$H[\cos(\varphi_f(t))] = \frac{1}{\pi} \int_{-\infty}^{+\infty} \frac{\cos(\varphi_f(\tau))}{t-\tau} d\tau. \quad (9)$$

If the Hilbert transform is written as the system response function $H(j\omega)=|H(j\omega)|e^{j\psi(\omega)}$, the following formulas can be obtained

$$|H(j\omega)|=1, \quad (10)$$

$$\psi(\omega) = \begin{cases} -\pi/2, & \omega > 0 \\ 0, & \omega = 0, \\ +\pi/2, & \omega < 0 \end{cases} \quad (11)$$

where $\psi(\omega)$ is the phase frequency response characteristic. From the above equation, it is obtained that when the phase function $\cos(\varphi(t))$ of the interference signal passes through the Hilbert transform, it can be seen as passing through an all-pass filter with amplitude 1. While the part of the signal with angular frequency $\omega > 0$ is phase shifted by $-\pi/2$, and the part of the signal with angular frequency $\omega < 0$ is phase shifted by $+\pi/2$. It can be obtained that the phase difference between the transformed signal and the original signal is $\pi/2$, and then the transformed interference signal is divided with the original signal to obtain the phase containing the microsphere motion information $\varphi'(t)$, as shown in Fig.7(c), but the amplitude of $\varphi'(t)$ obtained at this time is limited between $[-\pi, \pi]$, and in order to obtain the true phase amplitude $\varphi(t)$, it is necessary to expand $\varphi'(t)$, and finally, according to Eq.(8), the displacement curve of the motion of the sphere can be obtained, as shown in Fig.7(d), from which it can be seen that the maximum displacement of the cell is about $10.5 \mu\text{m}$ during the movement of the cell, it leads to a decelerated motion characteristic because the thrust force on the cell decreases with the increase of the distance.

Finally, to verify the reliability and stability of the method proposed in this paper, we continuously monitored 6 groups of particle tracks with different moving distances. The results are shown in Fig.8, indicating that the method has good applicability.

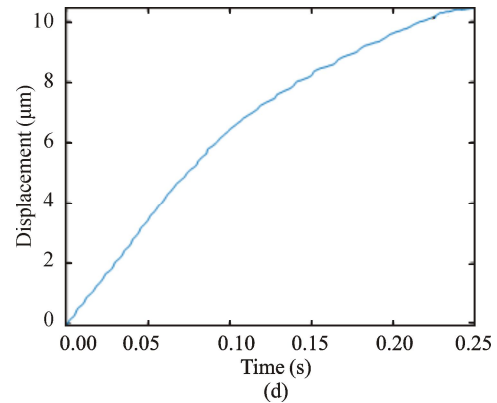
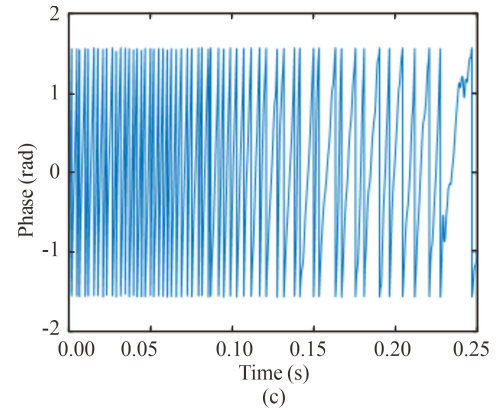
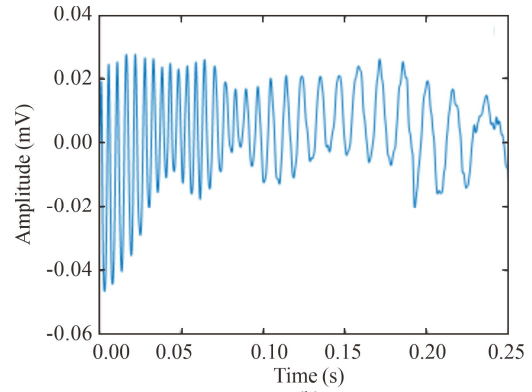


Fig.7 Schematic diagram of microsphere displacement reconstruction: (a) Original interference signal; (b) Filtered signal; (c) Demodulated phase signal; (d) Microsphere displacement curve

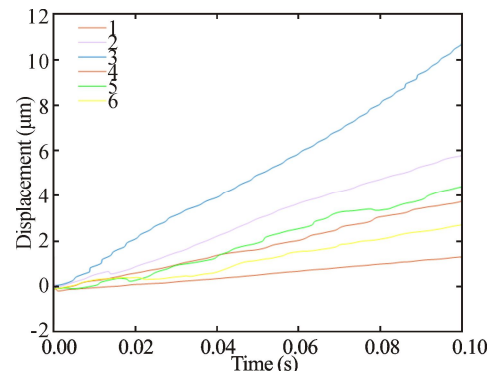
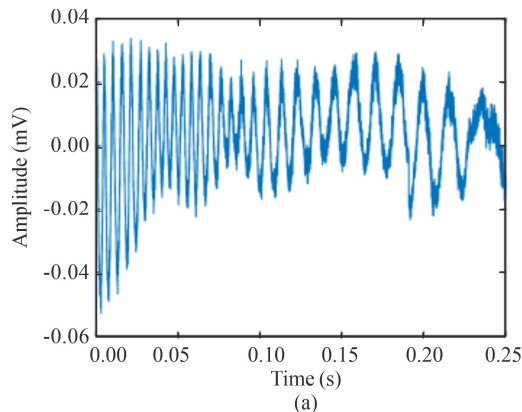


Fig.8 Schematic diagram of repeatability measurement results

In this paper, a tapered optical fiber sensor for detecting particle motion trajectory is proposed, the optical field distribution at the tip of the fiber after stretching is analyzed, and the magnitude of the force situation when the microspheres are at different positions of the tip of the tapered fiber is calculated using simulation software. Stable capture and transport of silica microspheres and yeast biological cells were achieved. On this basis, the interference signal due to particle motion was collected using the tapered optical fiber as a sensing element, and then the particle motion trajectory was mapped by demodulating the interference signal using Hilbert variation algorithm. The experimental results show that the method can effectively identify the velocity of particle motion as well as the farthest displacement of particle motion, and this work provides a potential technical detection means to realize the visualization of targeted drug delivery operations in biomedicine.

Ethics declarations

Conflicts of interest

The authors declare no conflict of interest.

References

- [1] ZHAO X T, ZHAO N, SHI Y, et al. Optical fiber tweezers: a versatile tool for optical trapping and manipulation[J]. *Micromachines*, 2020, 11(2): 114.
- [2] NORTON N M, FISCHER K J. Effects of micropipette handle diameter and inclusion of finger rest on basilar thumb joint contact mechanics[J]. *Medical engineering & physics*, 2023, 111: 103940.
- [3] WEINSTEIN T, GILON H, FILC O, et al. Automated manipulation of miniature objects underwater using air capillary bridges: pick-and-place, surface cleaning, and underwater origami[J]. *ACS applied materials & interfaces*, 2022, 14(7): 9855-9863.
- [4] XIA F Z, YOUCEF-TOUMI K. Review: advanced atomic force microscopy modes for biomedical research[J]. *Biosensors*, 2022, 12(12): 1116.
- [5] GAO B K, ZHONG H, YAN B, et al. Combined single/dual fiber optical trapping for flexible particle manipulation[J]. *Optics and lasers in engineering*, 2023, 161: 107373.
- [6] LIBERALE C, MINZIONI P, BRAGHERI F, et al. Miniaturized all-fibre probe for three-dimensional optical trapping and manipulation[J]. *Nature photonics*, 2007, 1(12): 723-727.
- [7] WU H, JIANG C L, TIAN S P, et al. Multifunctional single-fiber optical tweezers for particle trapping and transport[J]. *Chinese optics letters*, 2022, 20(12): 121201.
- [8] LIU Z, GUO C, YANG J, et al. Tapered fiber optical tweezers for microscopic particle trapping: fabrication and application[J]. *Optics express*, 2006, 14(25): 12510-12516.
- [9] MOHANTY S K, MOHANTY K, BERNS M W J J O B O. Manipulation of mammalian cells using a single-fiber optical microbeam[J]. *Journal of biomedical optics*, 2008, 13(5): 054049-054049-7.
- [10] ZHANG Y X, WANG C, ZHANG Y, et al. Single fiber optical tweezer for particles multi-dimensional arrangement[J]. *Journal of lightwave technology*, 2022, 40(4): 1144-1149.
- [11] ZHANG X T, YUAN T T, YANG S T, et al. Optical trajectory transport device based on a three-core fiber[J]. *Optics & laser technology*, 2021, 140: 107076.
- [12] PRYAMIKOV A, HADZIEVSKI L, FEDORUK M, et al. Optical vortices in waveguides with discrete and continuous rotational symmetry[J]. *Journal of the European Optical Society-rapid publications*, 2021, 17: 1-28.
- [13] ZHANG Z, LI C, HUANG Z J O C. Vibration measurement based on multiple Hilbert transform for self-mixing interferometry[J]. *Optics communications*, 2019, 436: 192-196.